
Rough Transformers: Lightweight Continuous-Time Sequence Modelling with Path Signatures

Fernando Moreno-Pino^{1,*}, Álvaro Arroyo^{1,2,*}, Harrison Waldon^{1,*},
 Xiaowen Dong^{1,2}, Álvaro Cartea^{1,3}

¹ Oxford-Man Institute, University of Oxford

² Machine Learning Research Group, University of Oxford

³ Mathematical Institute, University of Oxford

Abstract

Time-series data in real-world settings typically exhibit long-range dependencies and are observed at non-uniform intervals. In these settings, traditional sequence-based recurrent models struggle. To overcome this, researchers often replace recurrent architectures with Neural ODE-based models to account for irregularly sampled data and use Transformer-based architectures to account for long-range dependencies. Despite the success of these two approaches, both incur very high computational costs for input sequences of even moderate length. To address this challenge, we introduce the Rough Transformer, a variation of the Transformer model that operates on continuous-time representations of input sequences and incurs significantly lower computational costs. In particular, we propose *multi-view signature attention*, which uses path signatures to augment vanilla attention and to capture both local and global (multi-scale) dependencies in the input data, while remaining robust to changes in the sequence length and sampling frequency and yielding improved spatial processing. We find that, on a variety of time-series-related tasks, Rough Transformers consistently outperform their vanilla attention counterparts while obtaining the representational benefits of Neural ODE-based models, all at a fraction of the computational time and memory resources.

1 Introduction

Real-world sequential data in areas such as healthcare [67], finance [37], and biology [29] often are irregularly sampled, of variable length, and exhibit long-range dependencies. Furthermore, these data, which may be drawn from financial limit order books [9] or EEG readings [81], are often sampled at high frequency, yielding long sequences of data. Hence, many popular machine learning models struggle to model real-world sequential data, due to input dimension inflexibility, memory constraints, and computational bottlenecks. Rather than treating these data as *discrete* sequences, effective theoretical models often assume data are generated from some underlying *continuous-time* process [56, 68]. Hence, there is an increased interest in developing machine learning methods that use *continuous-time* representations to analyze sequential data.

One recent approach to modelling continuous-time data involves the development of continuous-time analogues of standard deep learning models, such as Neural ODEs [13] and Neural CDEs [48], which extend ResNets [38] and RNNs [31], respectively, to continuous-time settings. Instead of processing discrete data directly, these models operate on a latent continuous-time representation of input sequences. This approach is successful in continuous-time modelling tasks where standard

*Equal contribution.

Email: {fernando.moreno-pino, alvaro.arroyo, harrison.waldon}@eng.ox.ac.uk

deep recurrent models fail. In particular, extensions of vanilla Neural ODEs to the time-series setting [71, 48] succeed in various domains such as adaptive uncertainty quantification [62], counterfactual inference [77], or generative modelling [8].

In the meantime, in many practical settings, such as financial market volatility [22, 57] or heart rate fluctuations [36], continuous-time data also exhibit long-range dependencies. That is, data from the distant past may impact the system’s current behavior. Deep recurrent models struggle in this setting due to vanishing gradients. Several recent works [55, 61] successfully extract long-range dependencies from sequential data with Transformers [82], which learn temporal dependencies of a tokenized representation of input sequences. To extract such temporal dependencies requires a positional embedding of input data, because the attention mechanism is permutation invariant, which projects data into some latent space. The parallelizable nature of the Transformer allows for rapid training and evaluation on sequences of moderate length and it contributes to its success in fields such as natural language processing (NLP).

While the above approaches succeed in certain settings, several limitations hinder their wider applications. On the one hand, Neural ODEs and their analogues [48, 71] bear substantial computational costs when modelling long sequences of high dimension; see [60]. On the other hand, Transformers operate on discrete-time representations of input sequences, whose relative ordering is represented by the positional embedding. This representation may inhibit their expressivity in continuous-time data modelling tasks [88]. Moreover, Transformer-based models suffer from a number of difficulties: (i) input sequences must be sampled at the same times, (ii) the sequence length must be fixed, and (iii) the computational cost scales quadratically in the length of the input sequence. These difficulties severely limit the application of Transformers to continuous-time data modelling.

Contributions 1) We introduce *Rough Transformers*, a variant of the Transformer architecture amenable to the processing of continuous-time signals, which can be easily integrated into existing code-bases. The Rough Transformer is built upon the path signature from Rough Path Theory [53]. We define a novel, multi-scale transformation which projects discrete input data to a continuous-time path and compresses the input data with minimal information loss. Moreover, this transformation is an efficient feature representation of continuous-time paths, because linear functionals of path signatures approximate continuous functions of paths arbitrarily well (see Theorem A.2 in Appendix A).

2) We introduce the *multi-view attention mechanism* to extract both local and global dependencies of very long time-series efficiently. This mechanism operates directly on continuous-time representations of data without the need for expensive numerical solvers or constraints on the smoothness of the data stream. Moreover, the multi-view attention mechanism is provably robust to irregularly sampled data.

3) We carry out extensive experimentation on long and irregularly sampled time-series data. In particular, we show that Rough Transformers (i) improve the learning dynamics of the Transformer, making it more sample-efficient and allowing it to achieve better out-of-sample results, (ii) reduce the training cost by a factor of up to $25\times$ when compared with vanilla Transformers and more when compared with Neural ODE based architectures, (iii) maintain similar performance when data are irregularly sampled, where traditional recurrent-based models suffer a substantial decrease in performance [71], and (iv) yield improved spatial processing, accounting for relationships between different temporal channels without having to pre-define a specific inter-channel relation structure.

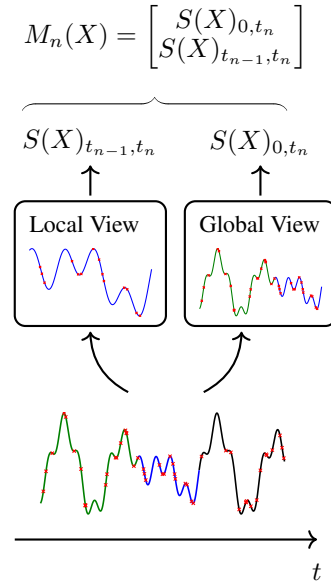


Figure 1: A representation of the multi-view signature. The continuous-time path is irregularly sampled at points marked with a red x . The local and global signatures of a linear interpolation of these points are computed and concatenated to form the multi-view signature. The multi-view signature transform consists of \bar{L} multi-view signatures.

2 Background and Methodology

Problem Formulation. In many real-world scenarios, sequential data are time-series sampled from some underlying continuous-time process, so datasets consist of long, irregularly sampled sequences of varied lengths. In these settings, the problem of sequence modelling is described as follows. Let $\hat{X} \in C(\mathbb{R}^+; \mathbb{R}^d)$ be a continuous-time *path*. A time-series of length L with sampling times $\mathcal{T}_{\mathbf{X}} = (t_1, \dots, t_n)$ is defined as $\mathbf{X} = ((t_0, X_0), \dots, (t_L, X_L))$, where $X_i = \hat{X}(t_i) \in \mathbb{R}^d$. Now, define a functional $f : C(\mathbb{R}^+; \mathbb{R}^d) \rightarrow \mathbb{R}^k$, where $C(\mathbb{R}^+; \mathbb{R}^d) = \{g : \mathbb{R}^+ \rightarrow \mathbb{R}^d \mid g \text{ continuous}\}$. Next define a dataset $\mathcal{D} = \left\{ (\mathbf{X}^i, f(\hat{X}^i))_{i=1}^N \right\}$. We seek to approximate the function f from the set \mathcal{D} for some downstream task. Importantly, we do not assume that $\mathcal{T}_{\mathbf{X}} = \mathcal{T}_{\mathbf{Y}}$ for all $\mathbf{X}, \mathbf{Y} \in \mathcal{D}$, so that \mathcal{D} may be irregularly sampled.

Sequence Modelling with Transformers. Transformers are used extensively as a baseline architecture to approximate functions of discrete-time sequential data and are successfully applied to settings when input sequences are fixed in length, relatively short, and sampled at regular intervals. First, the Transformer projects input time series $\mathbf{X} \in \mathbb{R}^{L \times d}$ to a high-dimensional space $\mathbf{X} \mapsto T(\mathbf{X}) \in \mathbb{R}^{L \times d'}$ for $d' \gg d$ using some linear positional encoding $T : \mathbb{R}^{L \times d} \rightarrow \mathbb{R}^{L \times d'}$. Next, a latent representation of the encoded sequence is learned by a multi-headed self-attention mechanism which splits $T(\mathbf{X})$ into H distinct query, key, and value sequences: $Q_h = T(\mathbf{X})W_h^Q$, $K_h = T(\mathbf{X})W_h^K$, $V_h = T(\mathbf{X})W_h^V$, respectively, with $h = 1, \dots, H$ and weight matrices $W_h^Q, W_h^K, W_h^V \in \mathbb{R}^{d' \times d}$. The multi-head self-attention calculation for each head is given by

$$O_h = \text{softmax} \left(\frac{Q_h K_h^\top}{\sqrt{d_k}} \right) V_h, \quad (1)$$

and the latent representation is projected to the output space \mathbb{R}^k using a multi-layer perceptron (MLP).

The input length L of the MLP and the Transformer is fixed by assumption. To evaluate the Transformer on a time-series \mathbf{X} with $|\mathcal{T}_{\mathbf{X}}| \neq n$, one must perform some transformation (interpolation, extrapolation, etc.) which may degrade the performance of the model. Furthermore, the memory and time complexity of the Transformer scales with $O(L^2)$, which presents a substantial difficulty in modelling long sequences.

Rough Path Signatures. Broadly, the difficulties faced by the Transformer in modelling time-series stem from time-series being sampled from underlying *continuous-time* objects, while the attention mechanism underpinning the Transformer is designed to model discrete sequences. To address these difficulties, Rough Transformers augment standard Transformers by lifting the input time-series to the space of continuous-time functions and performing the self-attention calculation in this infinite-dimensional space. To achieve this, we use the path signature from Rough Path Theory.

For a continuous-time path $\hat{X} \in C_b^1(\mathbb{R}^+; \mathbb{R}^d)$ and times $s, t \in \mathbb{R}^+$, the path signature of \hat{X} from s to t , denoted $S(\hat{X})_{s,t}$, is defined as follows. First, let

$$\mathcal{I}_d = \{(i_1, \dots, i_p) : i_j \in \{1, \dots, d\} \forall j \text{ and } p \in \mathbb{N}\} \quad (2)$$

denote the set of all d -multi-indices and $\mathcal{I}_d^n = \{I \in \mathcal{I}_d : |I| = n\}$. Next, set $S(\hat{X})_{s,t}^0 := 1$ and for any $I \in \mathcal{I}_d$, define

$$S(\hat{X})_{s,t}^I = \int_{s < u_1 < \dots < u_p < t} \dot{\hat{X}}^{i_1}(u_1) \cdots \dot{\hat{X}}^{i_p}(u_p) du_1 \dots du_p, \quad (3)$$

where $\dot{\hat{X}}^j = d\hat{X}^j/dt$. Abusing notation, define level n of the signature as

$$S^n(\hat{X})_{s,t} = \left\{ S(\hat{X})_{s,t}^I : I \in \mathcal{I}_d^n \right\}. \quad (4)$$

and define the signature as the infinite sequence

$$S(\hat{X})_{s,t}^n = (S(\hat{X})_{s,t}^0, S(\hat{X})_{s,t}^1, \dots, S(\hat{X})_{s,t}^n, \dots). \quad (5)$$

Finally, define the truncation of the signature $S(\widehat{X})_{s,t}^{\leq n} = (S(\widehat{X})_{s,t}^0, \dots, S(\widehat{X})_{s,t}^n)$, where $S(\widehat{X})_{s,t}^n$ can be interpreted as an element of the *extended tensor algebra* of \mathbb{R}^d :

$$T((\mathbb{R}^d)) = \{(a_0, \dots, a_n, \dots) : a_n \in \mathbb{R}^{d^{\otimes n}}\}. \quad (6)$$

Analogously, we say that $S(\widehat{X})_{s,t}^{\leq n} \in T((\mathbb{R}^d))_{\leq n}$. A central property of the signature is that is invariant with respect to time-reparameterization [53]. That is, let $\gamma : [0, T] \rightarrow [0, T]$ be surjective, continuous, and non-decreasing. Then we have

$$S(\widehat{X})_{0,T} = S(\widehat{X} \circ \gamma)_{0,T}, \quad (7)$$

which will be crucial to demonstrate the Rough Transformer’s robustness to irregularly sampled data.

In contrast to wavelets or Fourier transforms, which parameterize paths on a functional basis, the signature provides a basis for functions of continuous paths. Hence, the path signature is well-suited to sequence modelling tasks in which one seeks to learn a function of the underlying functional. For a more rigorous presentation of signatures and a description of additional properties, see Appendix A and Lyons et al. [53].

3 Rough Transformers

Now, we construct the Rough Transformer, a Transformer-based architecture that operates on continuous-time sequential data by means of the path signature.

Let \mathcal{D} be a dataset of irregularly sampled time-series. To project a discretized time-series $\mathbf{X} \in \mathcal{D}$ to a continuous-time object, let \tilde{X} denote the piecewise-linear interpolation of \mathbf{X} .² Next, for $t_k \in \mathcal{T}$, define the *multi-view signature*

$$M(\mathbf{X})_k := \left(S(\tilde{X})_{0,t_k}, S(\tilde{X})_{t_{k-1},t_k} \right). \quad (8)$$

In what follows, we refer to the components of $\left(S(\tilde{X})_{0,t_k}, S(\tilde{X})_{t_{k-1},t_k} \right)$ as *global* and *local*, respectively; see Figure 1. Intuitively, one can interpret the global component as an efficient representation of long-term information (see Theorem A.2 in Appendix A), and the local component as a type of convolutional filter that is invariant to the sampling rate of the signal. Now, define the *multi-view signature transform* $M(\mathbf{X}) = (M(\mathbf{X})_1, \dots, M(\mathbf{X})_{\bar{L}})$, and denote by $M(\mathbf{X})^{\leq n}$ the truncated signature for a truncation level n . Next, define the *multi-view attention mechanism*, which uses the multi-view signature transform to extend the standard attention mechanism to the space of continuous functions [53]. First, fix a truncation level $n \in \mathbb{N}$, and let $\bar{d} \in \mathbb{N}$ be such that $M(\mathbf{X})_k^{\leq n} \in \mathbb{R}^{\bar{d}}$. For $h = 1, \dots, H$ let $W_h^{\tilde{Q}, \tilde{K}, \tilde{V}} \in \mathbb{R}^{\bar{d} \times \bar{d}}$ for some $\bar{d}' \in \mathbb{N}$, and let

$$\tilde{Q}_h = M(\mathbf{X})^{\leq n} W_h^{\tilde{Q}}, \quad (9)$$

$$\tilde{K}_h = M(\mathbf{X})^{\leq n} W_h^{\tilde{K}}, \quad (10)$$

$$\tilde{V}_h = M(\mathbf{X})^{\leq n} W_h^{\tilde{V}}. \quad (11)$$

Then, the attention calculation is given by

$$O_h = \text{softmax} \left(\frac{\tilde{Q}_h \tilde{K}_h^\top}{\sqrt{\bar{d}'}} \right) \tilde{V}_h. \quad (12)$$

Notice that the attention calculation is similar to (1), however, we stress that the multi-view attention is built on *continuous-time* objects, the signatures, while the standard attention mechanism acts on discrete objects. The multi-view signature provides a compressed representation of the time series, minimizing the computational costs associated to quadratic scaling without excessive loss of representational capacity, see Appendix E.

²Any continuous-time interpolation of \mathbf{X} can be used, e.g., splines. However, the signature computation of piecewise-linear paths is particularly fast; see Appendix A.

3.1 Advantages of Rough Transformers

Computational Efficiency. As demonstrated below in Section 4, multi-view attention mechanism can substantially reduce the computational cost of vanilla Transformers. In particular, the attention calculation decreases from $O(L^2 d)$ in the vanilla case to $O(\bar{L}^2 d)$, where $\bar{L} \ll L$ with Rough Transformers. This enables both faster wall-clock training time and the ability to process long input sequences which would otherwise yield out-of-memory errors for the vanilla Transformer. Moreover, the multi-view attention mechanism does not require backpropagation through the signature calculation and can be computed *offline*. This is significantly more computationally efficient compared with the complexity of computing signatures batch-wise in every training step. Finally, the signature of piecewise-linear paths can be computed explicitly, see Appendix A, and there are a number of Python packages devoted to optimized signature calculation [46, 70].

Variable Length and Irregular Sampling. The multi-view signature transform underpinning Rough Transformers is evaluated by constructing a continuous-time interpolation of input data and computing a series of iterated integrals of this interpolation. The bounds of these integrals are a fixed set of time points, meaning that the sequence length of the multi-view attention mechanism is fixed and independent of the sequence length of input samples. Furthermore, the following proposition shows that the output of the Rough Transformer for two (possibly irregular) samplings of the same path is similar.

Proposition 3.1. *Let \mathbb{T} be a Rough Transformer. Suppose $\widehat{X} : [0, T] \rightarrow \mathbb{R}^d$ is a continuous-time process, and let $\gamma : [0, T] \rightarrow [0, T]$ denote a time-reparameterization. Suppose \mathbf{X} and \mathbf{X}' are samplings of \widehat{X} and $\widehat{X} \circ \gamma$, respectively. Then $\mathbb{T}(\mathbf{X}) \approx \mathbb{T}(\mathbf{X}')$.*

Proof. By (7), $S(\widehat{X})_{s,t} = S(\widehat{X} \circ \gamma)_{s,t}$ for all $s, t \in [0, T]$. Hence, one has $M(X^1) \approx M(X^2)$. Finally, $\mathbb{T}(X^1) \approx \mathbb{T}(X^2)$ because the attention mechanism and final MLP are both continuous. \square

Hence, the Rough Transformer is robust to irregular sampling. In many tasks, the sampling times convey important information about the time-series. In these settings, one may augment the input time-series with its sampling times, that is, write $X = ((t_0, X_0), \dots, (t_L, X_L))$.

Spatial Processing. While an interpolation of input data could be sampled to make vanilla Transformers independent of the length of the input sequence, important locality information could be lost, see Appendix E.2. Instead, Rough Transformers summarize spatial interactions between channels by means of the multi-view signature transform. One may notice that in (5), the dimension of the signature grows exponentially in the level of the signature n . In particular, when $X_i \in \mathbb{R}^d$, $|S(\tilde{X})_{0,t}^{\leq n}| = \frac{d(d^n-1)}{d-1} = O(d^n)$, so the multi-view attention calculation is of order $O(\bar{L}^2 d^n)$. In many practical time-series modelling problems, however, the value of d is not very large. The signature terms also decay factorially in the signature level n (see Proposition A.3 in Appendix A), so in practice, one may take the value of n to be small without sacrificing performance. The majority of computational savings result from the reduction of the sequence length to \bar{L} , and in practice, we take $\bar{L} \ll L$.

When the dimension d is large, there are three possible remedies to maintain computational efficiency. First, instead of computing the signature in $M(X)_k = (S(X)_{0,t_k}, S(\tilde{X})_{t_{k-1},t_k})$, one may compute the *log-signature*, which is a compressed version of the signature [69]. When the dimension is large enough such that the log-signature is computationally infeasible, one may instead compute the *univariate* signatures of features coupled with the time channel. That is, consider $\widehat{X} \in C([0, T]; \mathbb{R}^d)$, with $\widehat{X}(t) = (\widehat{X}_1(t), \dots, \widehat{X}_d(t))$. Denote the time-added function $\bar{X}_i(t) := (t, \widehat{X}_i(t))$. Then we define the *univariate multi-view signature*

$$\widehat{M}(\widehat{X})_k = (M(\bar{X}_1)_k, \dots, M(\bar{X}_d)_k). \quad (13)$$

The attention mechanism in this case is constructed as before. Fixing the maximum signature depth to be some value n^* , one sees that the number of features in the univariate multi-view signature is approximately $2^{n^*} d$. In practice we find that $n^* \leq 5$ provides sufficient performance, so the order of the attention calculation is $O(C \bar{L}^2 d)$ for $C \leq 2^{n^*}$. Finally, one may use randomized signatures to reduce dimension by using a Johnson-Lindenstrauss-type projection to a low-dimensional latent space and computing the signature in this space, as in [23, 21].

4 Experiments

In this section, we present empirical results which explore the effectiveness of the Rough Transformer, hereafter denoted RFormer, on a variety of time-series-related tasks. Experimental and hyperparameter details regarding the implementation of the method are in Appendices C and D. We consider long and multivariate time-series as our main experimental setting, because we expect signatures to perform best in this scenario. Additional experimentation on long-range reasoning tasks on image-based datasets is left for future work, as these would likely require additional inductive biases.

To benchmark RFormer, we select a variety of discrete-time and continuous-time sequence models. In particular, we include traditional gated RNN models (GRU [16]), ODE-based methods designed for sequential data (ODE-RNN [71] and Neural-CDE [48]), as well as ODE-based methods explicitly designed for long time-series (Neural-RDE [60]).³ Furthermore, we compare against a vanilla Transformer [82] with single-headed attention which is the RFormer backbone. Finally, we present comparisons with a recent continuous-time Transformer model, ContiFormer [14], to highlight the computational efficiency gap between RFormer and similar continuous-time models. See Appendix B for additional discussion on related models and more details about our experimental choices.

4.1 Results

Frequency Classification. Our first experiment is based on a set of synthetically generated time series from continuous paths of the form

$$\widehat{X}(t) = g(t) \sin(\omega t + \nu) + \eta(t), \quad (14)$$

where $g(t)$ is a non-linear trend component, ν and η are two noise terms, and ω is the frequency. Here, the task of the model is to classify the time-series according to its frequency ω . We consider 1000 samples in 100 classes with ω evenly distributed from 10 to 500. Each time-series is regularly sampled with 2000 times-steps on the interval $[0, 1]$. This synthetic experiment is similar to others in recent work on time-series modelling [51, 86, 58]. We include an additional experiment in which we alter the signal in (14) so its frequency is ω_0 for $t < t_0$ and ω_1 afterward, where the task is to classify the sinusoid based on the first frequency. We call this dataset the “long sinusoidal” dataset. This extension of the original experiment aims to test the ability of the model to perform long-range reasoning effectively.

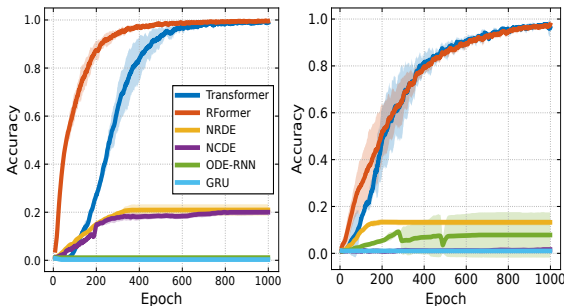


Figure 2: Test accuracy per epoch for the frequency classification task across three random seeds. **Left:** Sinusoidal dataset. **Right:** Long Sinusoidal dataset.

Figure 2 shows that RFormer improves the performance of the Transformer in two ways. First, the inclusion of both local and global information with the multi-view signature enhances the sample efficiency of the model, even though the attention mechanism is now operating on a much shorter sequence. Second, as seen in Table 4, the model is robust to changes in the sampling frequency at inference time, despite operating with half of the context. Therefore, in this task, unlike the vanilla Transformer, RFormer adapts to changes in both the length and the sampling frequency of the input stream.⁴

When compared with other models, we see that GRU and ODE-RNN fail to capture the information in the signal, and are not able to obtain any meaningful performance improvement throughout the training period. This highlights the shortcomings of most RNN-based models when processing sequences of moderate length, which are very common in real-world applications. Neural-CDE and Neural-RDE, which are tailor-made for

³We only benchmark Neural-CDE models in settings where time series are of relatively short length, due to the computational demands of this model for longer sequences.

⁴We highlight that the drop in performance is likely due to aliasing, i.e., the sampling rate is below the Nyquist rate, meaning that higher frequency signals cannot be appropriately represented with the number of data points available.

long-range time series modelling, can capture some useful dependencies in the time series but fall short compared with both vanilla Transformer and RFormer.

EigenWorms. The EigenWorms dataset [85] consists of 259 sequences, each of 17,984 time samples and 6 channels, which capture the movement patterns of different worm species. The primary objective is to classify each sequence as arising from a worm of either wild-type or one of four distinct mutant types. We employ the same training, validation, and testing data split ratios as in Morrill et al. [60], and report our results in Table 1. In the following, we denote with \diamond the results from Morrill et al. [60] and with \dagger our reproduction.⁵

As before, continuous-time models that are not tailored for long-time series fail to summarize the long-range information in the dataset, leading to significantly decreased performance. Neural-RDE can propagate information in the long-term past better as reported in Morrill et al. [60]. Both Transformer and ContiFormer cannot run within GPU memory due to their quadratic scaling in the length of the sequence. In contrast, RFormer can cheaply train on the same device (see Section 4.2 for details) due to its ability to take advantage of the parallel nature of GPU processing and compress the original time series, see Figure 3, without losing out on important spatial interactions and reporting a $\sim 20\%$ increase in performance over the second best model. We highlight that RFormer runs *faster* and is actually the *fastest* across all models, by several orders of magnitude in some cases.

Table 1: Test accuracy (mean \pm std) along with average seconds per epoch (S/E), computed across five seeds on the EigenWorms dataset. The results correspond to both our reproduction and those presented in Morrill et al. [60].

Model	Eigenworms	
	Accuracy (%) \uparrow	S/E (sec.) \downarrow
ODE-RNN \diamond	47.9 \pm 5.3	-
Neural CDE \diamond	66.7 \pm 11.8	-
Neural RDE \diamond	83.8 \pm 3.0	-
GRU \dagger	38.50 \pm 10.1	0.25
ODE-RNN \dagger	37.61 \pm 2.42	48.59
Neural RDE \dagger	69.23 \pm 5.54	5.23
Transformer	OOM	-
ContiFormer	OOM	-
RFormer	90.24 \pm 2.15	0.11

importance of efficiently processing long time-series in practical applications. RNN-based models (GRU, ODE-RNN) achieve decent performance with both medium and long context windows, despite their problems with vanishing and exploding gradients. In this task, Neural-RDE performs poorly. This is likely because Neural-RDE computes the signature over all channels, which is ineffective in this context. The Transformer and RFormer models report the best performance. Also, the

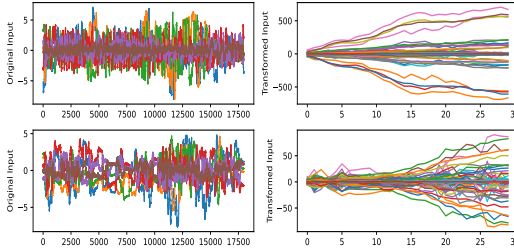


Figure 3: Original and hidden representation after signature layer for two examples in the EW dataset, achieving a $600\times$ compression rate in the temporal dimension. **Left:** Original time series. **Right:** Signature representation.

Time-to-cancellation of limit orders. We use limit order book data provided by LOBSTER [42] and test each model’s capacity to calculate the time-to-cancellation of 1000 limit orders of the AMZN ticker over a single trading day. We employ context windows of 1000 time-steps and 20000 time-steps in the past to make the prediction. Raw limit order book data consist of many uninformative samples [4], so one expects a longer context window would provide more information to make the prediction. However, this cannot be guaranteed given the non-stationarity and low SNR of financial environments [see 3, 4, 76]. Limit order book updates are not regularly sampled, even though they are obtained at a high sampling rate. Since this is a dataset with a higher number of features, we employ the univariate multi-view signature transform to avoid excessive growth with signature level. Table 2 shows that a longer context yields improved performance in this task, highlighting the im-

⁵We use our own reproduction to test the performance of all models in irregularly sampled datasets, which are not included in the original paper from Morrill et al. [60]. Random dropping requires window sizes larger than 2, because signatures cannot be computed over a single point. The next best step size was chosen in accordance with performance on the validation dataset, see Appendix D.

computational time and the performance of the model improves with univariate signatures in this context as well.

Table 2: Test RMSE (mean \pm std) and average seconds per epoch (S/E), computed across five seeds on the LOB dataset, on a scale of 10^{-2} .

Model	LOB - 1k Context Window		LOB - 20k Context Window	
	RMSE \downarrow	S/E (sec.) \downarrow	RMSE \downarrow	S/E (sec.) \downarrow
GRU	78.26 \pm 0.52	<u>0.05</u>	55.70 \pm 0.97	<u>0.61</u>
ODE-RNN	64.31 \pm 10.16	2.66	<u>56.48</u> \pm 0.99	50.71
Neural CDE	80.73 \pm 1.49	4.92	-	-
Neural RDE	110.41 \pm 18.68	12.00	78.06 \pm 7.09	118.40
Transformer	<u>39.15</u> \pm 0.13	0.07	OOM	-
ContiFormer	OOM	-	OOM	-
RFormer	38.81 \pm 0.19	0.04	38.44 \pm 0.15	0.07

HR dataset. Next, we consider the Heart Rate dataset from the TSR archive [80], originally sourced from Beth Israel Deaconess Medical Center (BIDMC). This dataset consists of time-series sampled from patient ECG readings, and each model is tasked with forecasting the patient’s heart rate (HR) at the sample’s conclusion. The data, sampled at 125Hz, consists of three-channel time-series (including time), each spanning 4000 time steps. We used the L2 loss metric to assess the performance. Table 3 shows the results.

The sequences in the HR dataset are sufficiently short to remain within memory when running the Transformer model. The baseline Transformer model improves over GRU, and ODE-RNN, however, it is less competitive when compared with Neural-RDE, suggesting that the Transformer is not particularly well-suited for this type of task. However, the RFormer model improves over the baseline Transformer by 67% and yields the best performance overall. Across all tasks, we see significant improvements in efficiency as a consequence of the signature computation. We elaborate on this in more detail in the following subsection.

4.2 Training Efficiency

Here, we focus on the computational gains of the model when compared with vanilla Transformers and methods that require numerical ODE solvers.

Attention-based architectures are highly parallelizable on modern GPUs, as opposed to traditional RNN models which require sequential updating. However, vanilla attention experiences a bottleneck in memory and time complexity as the sequence length L grows.

As covered above in Section 3, variations of the signature transform allow the model to operate on a reduced sequence length \bar{L} without increasing the dimensionality in a way that would become problematic for the model. This allows us to bypass the quadratic complexity of the model without resorting to sparsity techniques commonly used in the literature [27, 51].

Tables 1-3 shows that RFormer is competitive when modelling datasets with extremely long sequences (such as EW and the long LOB dataset) without an explosion in the memory requirements. RFormer exploits the parallelism of the attention mechanism to significantly accelerate training time, as the length of the input sequence is decreased substantially. In particular, we observe speedups of $1.4\times$ to $26.11\times$ with respect to standard attention, and higher when compared with all methods requiring numerical solutions to ODEs. The computational efficiency gains of RFormer are attained due to the signature transform reducing the length of the time-series with minimal information loss. The effectiveness of this transformation can be seen from the ablation study carried out in Appendix E.

Table 3: Test RMSE (mean \pm std) and average seconds per epoch (S/E), computed across five seeds on the Heart Rate (HR) dataset. The results correspond to both our reproduction and those presented in [60].

Model	HR	
	RMSE \downarrow	S/E (sec.) \downarrow
ODE-RNN $^\diamond$	13.06 \pm 0.00	-
Neural CDE $^\diamond$	9.82 \pm 0.34	-
Neural RDE $^\diamond$	2.97 \pm 0.45	-
GRU †	13.06 \pm 0.00	<u>1.07</u>
ODE-RNN †	13.06 \pm 0.00	50.71
Neural RDE †	4.04 \pm 0.11	9.52
Transformer	8.24 \pm 2.24	11.71
ContiFormer	OOM	-
RFormer	2.66 \pm 0.21	0.45

This contrasts with NRDEs [60], which augment NCDEs with local signatures of input data, and find that smaller windows often perform better. Furthermore, NRDEs do not experience the same computational gains as RFormer because they must perform many costly ODE integration steps.

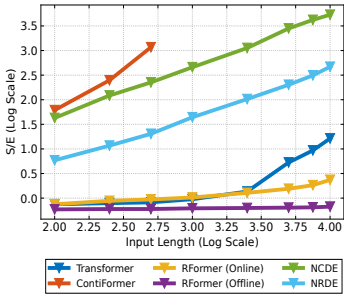


Figure 4: Seconds per epoch for growing input length (on a log-log scale) and for different model types on the sinusoidal dataset.

machine. In addition to improved computational performance, we demonstrate in the subsequent sections that RFormer is empirically robust to irregularly sampled observations and is able to capture spatial interactions better. Finally, in Appendix B we elaborate on how approximations of the self-attention matrix could be added to our framework, and Appendix F includes additional experiments on the computational efficiency of RFormer for extremely long sequences (up to $L = 250K$).

4.3 Irregular sampling

So far, we mainly focused on the efficiency and inductive bias afforded to the model through the use of signatures. However, a key element of RFormer is that it can naturally deal with irregularly sampled sequences without expensive numerical ODE solvers. This property follows from the fact that signatures are *invariant to time reparameterization*, see Proposition 3.1. In this subsection, we empirically test this property by training the model on the same datasets but randomly dropping 50% of the points at every epoch. This test intends to find if the model is able to learn continuous-time representations of the original input time-series. The results can be found in Table 4. We find that RFormer consistently results in the best performance, with a small performance drop when compared to the full dataset. Importantly, this property is achieved in conjunction with the efficiency gains afforded to the model and without the use of expensive numerical ODE solvers. For more details and more exhaustive experimentation on random data drops, see Appendix F.

Table 4: Performance of all models under a random 50% drop in datapoints per epoch.

Model	50% Drop Performance			
	EW (%) \uparrow	HR \downarrow	Sine (%) \uparrow	Sine Long (%) \uparrow
GRU	35.90	13.06	0.96	1.16
ODE-RNN	37.61	13.06	1.06	1.23
Neural RDE	<u>60.68</u>	<u>4.67</u>	0.94	0.87
Transformer	OOM	12.73	<u>7.37</u>	<u>20.23</u>
RFormer	87.69	2.96	59.57	93.17

randomly dropping 50% of the points at every epoch. This test intends to find if the model is able to learn continuous-time representations of the original input time-series. The results can be found in Table 4. We find that RFormer consistently results in the best performance, with a small performance drop when compared to the full dataset. Importantly, this property is achieved in conjunction with the efficiency gains afforded to the model and without the use of expensive numerical ODE solvers. For more details and more exhaustive experimentation on random data drops, see Appendix F.

4.4 Spatial Processing

Finally, we highlight that one of the reasons the model can achieve significant compression benefits (such as those in Figure 3) in the tasks considered is a consequence of its ability to *jointly* account for temporal and spatial interactions through the self-attention mechanism and signature terms, respectively. To highlight this, we run an additional experiment that can be found in Appendix F.

5 Conclusion

We introduced the Rough Transformer, a variant of the original Transformer that allows the processing of discrete-time series as continuous-time signals through the use of multi-view signature attention. Empirical comparisons showed that Rough Transformers outperform vanilla Transformers and continuous-time models on a variety of time-series tasks and are robust to the sampling rate of the

In Figure 4, we showcase the improvements in computational efficiency of RFormer compared to vanilla Transformers [82], continuous-time Transformers [14], and other continuous-time RNNs [48, 60] when processing sequences from $L = 100$ samples up to $L = 10K$. As seen, RFormer is significantly more efficient than its continuous-time and vanilla counterparts, even when performing the signature computation online, which involves computing the signatures for each batch during training, resulting in significant redundant computation. When signatures are pre-computed just once before training, the computational time of each epoch remains *constant* across input all sequence lengths including $L = 10K$ (see more details in Appendix F). Furthermore, we highlight that ContFormer has a sample complexity of $\mathcal{O}(L^2 d^2 S)$, where S represents the normalized number of function evaluations of the numerical ODE solver, which makes ContFormer orders of magnitude more computationally intensive when compared to RFormer and prevents the model from running on sequences longer than 500 points without running out of memory on our

signal. Finally, we showed that RFormer provides significant speedups in training time compared to regular attention and ODE-based methods, without the need for major architectural modifications or sparsity constraints.

Impact Statement

This paper introduces advancements in time series analysis, with implications across various sectors like finance, healthcare, and environmental monitoring. Our work enhances decision-making by providing more accurate and efficient methods to analyze time-series data. Positive impacts include improved financial market predictions, early disease detection in healthcare, and better environmental forecasting. However, we acknowledge potential misuses, such as unfair advantages in financial trading or privacy concerns in healthcare, and advocate for ethical application and regulatory oversight. Although our research primarily advances technical methodologies in machine learning, its societal impact merits careful consideration. We encourage responsible use of our methods.

Acknowledgements

We thank Christopher Salvi, Antonio Orvieto, Yannick Limmer and Benjamin Walker for discussions at different stages of the project. AA acknowledges support from the Rafael Del Pino Foundation.

References

- [1] M. Arjovsky, A. Shah, and Y. Bengio. Unitary evolution recurrent neural networks. In *International conference on machine learning*, pages 1120–1128. PMLR, 2016.
- [2] I. P. Arribas. Derivatives pricing using signature payoffs. *arXiv preprint arXiv:1809.09466*, 2018.
- [3] A. Arroyo, B. Scalzo, L. Stanković, and D. P. Mandic. Dynamic portfolio cuts: A spectral approach to graph-theoretic diversification. In *ICASSP 2022-2022 IEEE International Conference on Acoustics, Speech and Signal Processing (ICASSP)*, pages 5468–5472. IEEE, 2022.
- [4] A. Arroyo, A. Cartea, F. Moreno-Pino, and S. Zohren. Deep attentive survival analysis in limit order books: Estimating fill probabilities with convolutional-transformers. *Quantitative Finance*, pages 1–23, 2024.
- [5] I. Beltagy, M. E. Peters, and A. Cohan. Longformer: The long-document transformer. *arXiv preprint arXiv:2004.05150*, 2020.
- [6] M. Biloš, J. Sommer, S. S. Rangapuram, T. Januschowski, and S. Günnemann. Neural flows: Efficient alternative to neural odes. In M. Ranzato, A. Beygelzimer, Y. Dauphin, P. Liang, and J. W. Vaughan, editors, *Advances in Neural Information Processing Systems*, volume 34, pages 21325–21337. Curran Associates, Inc., 2021. URL https://proceedings.neurips.cc/paper_files/paper/2021/file/b21f9f98829dea9a48fd8aaddc1f159d-Paper.pdf.
- [7] H. S. d. O. Borde, Á. Arroyo, and I. Posner. Projections of model spaces for latent graph inference. *arXiv preprint arXiv:2303.11754*, 2023.
- [8] S. Calvo-Ordóñez, J. Huang, L. Zhang, G. Yang, C.-B. Schonlieb, and A. I. Aviles-Rivero. Beyond u: Making diffusion models faster & lighter. *arXiv preprint arXiv:2310.20092*, 2023.
- [9] Á. Cartea, S. Jaimungal, and J. Penalva. *Algorithmic and high-frequency trading*. Cambridge University Press, 2015.
- [10] Á. Cartea, G. Duran-Martin, and L. Sánchez-Betancourt. Detecting toxic flow. *arXiv preprint arXiv:2312.05827*, 2023.
- [11] B. Chang, M. Chen, E. Haber, and E. H. Chi. Antisymmetricrnn: A dynamical system view on recurrent neural networks. In *International Conference on Learning Representations*, 2018.
- [12] P. Chang, G. Durán-Martín, A. Y. Shestopaloff, M. Jones, and K. Murphy. Low-rank extended kalman filtering for online learning of neural networks from streaming data. *arXiv preprint arXiv:2305.19535*, 2023.
- [13] R. T. Chen, Y. Rubanova, J. Bettencourt, and D. K. Duvenaud. Neural ordinary differential equations. *Advances in neural information processing systems*, 31, 2018.
- [14] Y. Chen, K. Ren, Y. Wang, Y. Fang, W. Sun, and D. Li. Contiformer: Continuous-time transformer for irregular time series modeling. In *Thirty-seventh Conference on Neural Information Processing Systems*, 2023.
- [15] R. Child, S. Gray, A. Radford, and I. Sutskever. Generating long sequences with sparse transformers. *arXiv preprint arXiv:1904.10509*, 2019.
- [16] K. Cho, B. Van Merriënboer, C. Gulcehre, D. Bahdanau, F. Bougares, H. Schwenk, and Y. Bengio. Learning phrase representations using rnn encoder-decoder for statistical machine translation. *arXiv preprint arXiv:1406.1078*, 2014.
- [17] K. M. Choromanski, V. Likhoshesterov, D. Dohan, X. Song, A. Gane, T. Sarlos, P. Hawkins, J. Q. Davis, A. Mohiuddin, L. Kaiser, et al. Rethinking attention with performers. In *International Conference on Learning Representations*, 2020.
- [18] A. Cini, I. Marisca, and C. Alippi. Filling the g_{ap}s: Multivariate time series imputation by graph neural networks. In *International Conference on Learning Representations*, 2021.

- [19] A. Cini, I. Marisca, D. Zambon, and C. Alippi. Taming local effects in graph-based spatiotemporal forecasting. *Advances in Neural Information Processing Systems*, 36, 2024.
- [20] N. M. Cirone, A. Orvieto, B. Walker, C. Salvi, and T. Lyons. Theoretical foundations of deep selective state-space models. *arXiv preprint arXiv:2402.19047*, 2024.
- [21] E. M. Compagnoni, A. Scampicchio, L. Biggio, A. Orvieto, T. Hofmann, and J. Teichmann. On the effectiveness of randomized signatures as reservoir for learning rough dynamics. In *2023 International Joint Conference on Neural Networks (IJCNN)*, pages 1–8. IEEE, 2023.
- [22] F. Corsi. A simple approximate long-memory model of realized volatility. *Journal of Financial Econometrics*, 7(2):174–196, 2009.
- [23] C. Cuchiero, L. Gonon, L. Grigoryeva, J.-P. Ortega, and J. Teichmann. Discrete-time signatures and randomness in reservoir computing. *IEEE Transactions on Neural Networks and Learning Systems*, 33(11):6321–6330, 2021.
- [24] T. Dao, D. Fu, S. Ermon, A. Rudra, and C. Ré. Flashattention: Fast and memory-efficient exact attention with io-awareness. *Advances in Neural Information Processing Systems*, 35: 16344–16359, 2022.
- [25] E. Dupont, A. Doucet, and Y. W. Teh. Augmented neural odes. *Advances in neural information processing systems*, 32, 2019.
- [26] N. B. Erichson, O. Azencot, A. Queiruga, L. Hodgkinson, and M. W. Mahoney. Lipschitz recurrent neural networks. In *International Conference on Learning Representations*, 2020.
- [27] A. Feng, I. Li, Y. Jiang, and R. Ying. Diffuser: efficient transformers with multi-hop attention diffusion for long sequences. In *Proceedings of the AAAI Conference on Artificial Intelligence*, volume 37, pages 12772–12780, 2023.
- [28] A. Fermanian. Embedding and learning with signatures. *Computational Statistics & Data Analysis*, 157:107148, 2021.
- [29] C. Fleming, D. Sheldon, W. Fagan, P. Leimgruber, T. Mueller, D. Nandintsetseg, M. Noonan, K. Olson, E. Setyawan, A. Sianipar, et al. Correcting for missing and irregular data in home-range estimation. *Ecological Applications*, 28(4):1003–1010, 2018.
- [30] E. Fons, A. Sztrajman, Y. El-Laham, A. Iosifidis, and S. Vyetrenko. Hypertime: Implicit neural representation for time series. *arXiv preprint arXiv:2208.05836*, 2022.
- [31] K.-i. Funahashi and Y. Nakamura. Approximation of dynamical systems by continuous time recurrent neural networks. *Neural networks*, 6(6):801–806, 1993.
- [32] A. Gu and T. Dao. Mamba: Linear-time sequence modeling with selective state spaces. *arXiv preprint arXiv:2312.00752*, 2023.
- [33] A. Gu, K. Goel, and C. Re. Efficiently modeling long sequences with structured state spaces. In *International Conference on Learning Representations*, 2021.
- [34] B. Hambly and T. Lyons. Uniqueness for the signature of a path of bounded variation and the reduced path group. *Annals of Mathematics*, pages 109–167, 2010.
- [35] R. Hasani, M. Lechner, A. Amini, D. Rus, and R. Grosu. Liquid time-constant networks. In *Proceedings of the AAAI Conference on Artificial Intelligence*, volume 35, pages 7657–7666, 2021.
- [36] J. M. Hausdorff and C.-K. Peng. Multiscaled randomness: A possible source of 1/f noise in biology. *Physical review E*, 54(2):2154, 1996.
- [37] N. Hautsch. *Modelling irregularly spaced financial data: theory and practice of dynamic duration models*. Springer Science & Business Media, 2004.

- [38] K. He, X. Zhang, S. Ren, and J. Sun. Deep residual learning for image recognition. In *Proceedings of the IEEE conference on computer vision and pattern recognition*, pages 770–778, 2016.
- [39] M. Henaff, A. Szlam, and Y. LeCun. Recurrent orthogonal networks and long-memory tasks. In *International Conference on Machine Learning*, pages 2034–2042. PMLR, 2016.
- [40] M. Höglund, E. Ferrucci, C. Hernández, A. M. Gonzalez, C. Salvi, L. Sánchez-Betancourt, and Y. Zhang. A neural rde approach for continuous-time non-markovian stochastic control problems. In *ICML Workshop on New Frontiers in Learning, Control, and Dynamical Systems*, 2023.
- [41] S. I. Holt, Z. Qian, and M. van der Schaar. Neural laplace: Learning diverse classes of differential equations in the laplace domain. In *International Conference on Machine Learning*, pages 8811–8832. PMLR, 2022.
- [42] R. Huang and T. Polak. Lobster: Limit order book reconstruction system. *Available at SSRN 1977207*, 2011.
- [43] A. Katharopoulos, A. Vyas, N. Pappas, and F. Fleuret. Transformers are rnns: Fast autoregressive transformers with linear attention. In *International conference on machine learning*, pages 5156–5165. PMLR, 2020.
- [44] A. Kazi, L. Cosmo, S.-A. Ahmadi, N. Navab, and M. M. Bronstein. Differentiable graph module (dgm) for graph convolutional networks. *IEEE Transactions on Pattern Analysis and Machine Intelligence*, 45(2):1606–1617, 2022.
- [45] T. A. Keller, L. Muller, T. Sejnowski, and M. Welling. Traveling waves encode the recent past and enhance sequence learning. In *The Twelfth International Conference on Learning Representations*, 2023.
- [46] P. Kidger and T. Lyons. Signatory: differentiable computations of the signature and logsignature transforms, on both cpu and gpu. *arXiv preprint arXiv:2001.00706*, 2020.
- [47] P. Kidger, P. Bonnier, I. Perez Arribas, C. Salvi, and T. Lyons. Deep signature transforms. In H. Wallach, H. Larochelle, A. Beygelzimer, F. d'Alché-Buc, E. Fox, and R. Garnett, editors, *Advances in Neural Information Processing Systems*, volume 32. Curran Associates, Inc., 2019. URL https://proceedings.neurips.cc/paper_files/paper/2019/file/d2cdf047a6674cef251d56544a3cf029-Paper.pdf.
- [48] P. Kidger, J. Morrill, J. Foster, and T. Lyons. Neural controlled differential equations for irregular time series. *Advances in Neural Information Processing Systems*, 33:6696–6707, 2020.
- [49] M. Lemerrier, C. Salvi, T. Cass, E. V. Bonilla, T. Damoulas, and T. J. Lyons. Siggpde: Scaling sparse gaussian processes on sequential data. In *International Conference on Machine Learning*, pages 6233–6242. PMLR, 2021.
- [50] M. Lezcano-Casado and D. Martínez-Rubio. Cheap orthogonal constraints in neural networks: A simple parametrization of the orthogonal and unitary group. In *International Conference on Machine Learning*, pages 3794–3803. PMLR, 2019.
- [51] S. Li, X. Jin, Y. Xuan, X. Zhou, W. Chen, Y.-X. Wang, and X. Yan. Enhancing the locality and breaking the memory bottleneck of transformer on time series forecasting. *Advances in neural information processing systems*, 32, 2019.
- [52] Z. Li, N. B. Kovachki, K. Azizzadenesheli, K. Bhattacharya, A. Stuart, A. Anandkumar, et al. Fourier neural operator for parametric partial differential equations. In *International Conference on Learning Representations*, 2020.
- [53] T. J. Lyons, M. Caruana, and T. Lévy. *Differential equations driven by rough paths*. Springer, 2007.
- [54] I. Marisca, C. Alippi, and F. M. Bianchi. Graph-based forecasting with missing data through spatiotemporal downsampling. *arXiv preprint arXiv:2402.10634*, 2024.

- [55] V. Melnychuk, D. Frauen, and S. Feuerriegel. Causal transformer for estimating counterfactual outcomes. In *International Conference on Machine Learning*, pages 15293–15329. PMLR, 2022.
- [56] M. Morariu-Patrichi and M. S. Pakkanen. State-dependent hawkes processes and their application to limit order book modelling. *Quantitative Finance*, 22(3):563–583, 2022.
- [57] F. Moreno-Pino and S. Zohren. Deepvol: Volatility forecasting from high-frequency data with dilated causal convolutions. *arXiv preprint arXiv:2210.04797*, 2022.
- [58] F. Moreno-Pino, P. M. Olmos, and A. Artés-Rodríguez. Deep autoregressive models with spectral attention. *Pattern Recognition*, 133:109014, 2023.
- [59] F. Moreno-Pino, Á. Arroyo, H. Waldon, X. Dong, and Á. Cartea. Rough transformers for continuous and efficient time-series modelling. *arXiv preprint arXiv:2403.10288*, 2024.
- [60] J. Morrill, C. Salvi, P. Kidger, and J. Foster. Neural rough differential equations for long time series. In *International Conference on Machine Learning*, pages 7829–7838. PMLR, 2021.
- [61] T. Nguyen and A. Grover. Transformer neural processes: Uncertainty-aware meta learning via sequence modeling. In *International Conference on Machine Learning*, pages 16569–16594. PMLR, 2022.
- [62] A. Norcliffe, C. Bodnar, B. Day, J. Moss, and P. Liò. Neural ode processes. In *International Conference on Learning Representations*, 2020.
- [63] A. Norcliffe, C. Bodnar, B. Day, N. Simidjievski, and P. Liò. On second order behaviour in augmented neural odes. *Advances in neural information processing systems*, 33:5911–5921, 2020.
- [64] A. Orvieto, S. L. Smith, A. Gu, A. Fernando, C. Gulcehre, R. Pascanu, and S. De. Resurrecting recurrent neural networks for long sequences. In *International Conference on Machine Learning*, pages 26670–26698. PMLR, 2023.
- [65] Y. Park, J. Choi, C. Yoon, M. Kang, et al. Learning pde solution operator for continuous modeling of time-series. *arXiv preprint arXiv:2302.00854*, 2023.
- [66] I. Perez Arribas, G. M. Goodwin, J. R. Geddes, T. Lyons, and K. E. Saunders. A signature-based machine learning model for distinguishing bipolar disorder and borderline personality disorder. *Translational psychiatry*, 8(1):274, 2018.
- [67] S. Perveen, M. Shahbaz, T. Saba, K. Keshavjee, A. Rehman, and A. Guergachi. Handling irregularly sampled longitudinal data and prognostic modeling of diabetes using machine learning technique. *IEEE Access*, 8:21875–21885, 2020.
- [68] R. Ratcliff, P. L. Smith, S. D. Brown, and G. McKoon. Diffusion decision model: Current issues and history. *Trends in cognitive sciences*, 20(4):260–281, 2016.
- [69] J. Reizenstein. Calculation of iterated-integral signatures and log signatures. *arXiv preprint arXiv:1712.02757*, 2017.
- [70] J. Reizenstein and B. Graham. The iisignature library: efficient calculation of iterated-integral signatures and log signatures. *arXiv preprint arXiv:1802.08252*, 2018.
- [71] Y. Rubanova, R. T. Chen, and D. K. Duvenaud. Latent ordinary differential equations for irregularly-sampled time series. *Advances in neural information processing systems*, 32, 2019.
- [72] T. K. Rusch and S. Mishra. Coupled oscillatory recurrent neural network (cornn): An accurate and (gradient) stable architecture for learning long time dependencies. In *International Conference on Learning Representations*, 2020.
- [73] T. K. Rusch and S. Mishra. Unicornn: A recurrent model for learning very long time dependencies. In *International Conference on Machine Learning*, pages 9168–9178. PMLR, 2021.

- [74] T. K. Rusch, S. Mishra, N. B. Erichson, and M. W. Mahoney. Long expressive memory for sequence modeling. In *International Conference on Learning Representations*, 2021.
- [75] C. Salvi, M. Lemerrier, C. Liu, B. Horvath, T. Damoulas, and T. Lyons. Higher order kernel mean embeddings to capture filtrations of stochastic processes. *Advances in Neural Information Processing Systems*, 34:16635–16647, 2021.
- [76] B. Scalzo, A. Arroyo, L. Stanković, and D. P. Mandic. Nonstationary portfolios: Diversification in the spectral domain. In *ICASSP 2021-2021 IEEE International Conference on Acoustics, Speech and Signal Processing (ICASSP)*, pages 5155–5159. IEEE, 2021.
- [77] N. Seedat, F. Imrie, A. Bellot, Z. Qian, and M. van der Schaar. Continuous-time modeling of counterfactual outcomes using neural controlled differential equations. In *International Conference on Machine Learning*, pages 19497–19521. PMLR, 2022.
- [78] V. Sitzmann, J. Martel, A. Bergman, D. Lindell, and G. Wetzstein. Implicit neural representations with periodic activation functions. *Advances in neural information processing systems*, 33: 7462–7473, 2020.
- [79] C. Tallec and Y. Ollivier. Can recurrent neural networks warp time? *arXiv preprint arXiv:1804.11188*, 2018.
- [80] C. W. Tan, C. Bergmeir, F. Petitjean, and G. I. Webb. Monash university, uea, ucr time series extrinsic regression archive. *arXiv preprint arXiv:2006.10996*, 2020.
- [81] A. Vahid, M. Mückschel, S. Stober, A.-K. Stock, and C. Beste. Applying deep learning to single-trial eeg data provides evidence for complementary theories on action control. *Communications biology*, 3(1):112, 2020.
- [82] A. Vaswani, N. Shazeer, N. Parmar, J. Uszkoreit, L. Jones, A. N. Gomez, Ł. Kaiser, and I. Polosukhin. Attention is all you need. *Advances in neural information processing systems*, 30, 2017.
- [83] B. Walker, A. D. McLeod, T. Qin, Y. Cheng, H. Li, and T. Lyons. Log neural controlled differential equations: The lie brackets make a difference. *arXiv preprint arXiv:2402.18512*, 2024.
- [84] S. Wang, B. Z. Li, M. Khabsa, H. Fang, and H. Ma. Linformer: Self-attention with linear complexity. *arXiv preprint arXiv:2006.04768*, 2020.
- [85] E. Yemini, T. Jucikas, L. J. Grundy, A. E. Brown, and W. R. Schafer. A database of caenorhabditis elegans behavioral phenotypes. *Nature methods*, 10(9):877–879, 2013.
- [86] J. Yoon, D. Jarrett, and M. Van der Schaar. Time-series generative adversarial networks. *Advances in neural information processing systems*, 32, 2019.
- [87] M. Zaheer, G. Guruganesh, K. A. Dubey, J. Ainslie, C. Albeti, S. Ontanon, P. Pham, A. Ravula, Q. Wang, L. Yang, et al. Big bird: Transformers for longer sequences. *Advances in neural information processing systems*, 33:17283–17297, 2020.
- [88] A. Zeng, M. Chen, L. Zhang, and Q. Xu. Are transformers effective for time series forecasting? In *Proceedings of the AAAI conference on artificial intelligence*, volume 37, pages 11121–11128, 2023.

A Properties of Path Signatures

First, we recall that the path is uniquely determined by its signature, which motivates its use as a feature map.

Proposition A.1. *Given a path $\widehat{X} : [0, T] \rightarrow \mathbb{R}^d$, then the map $P : [0, T] \rightarrow \mathbb{R}^{1+d}$ where $P(t) = (t, \widehat{X}(t))$ is uniquely determined by its signature $S(P)_{0,T}$.*

The proof can be found in Hambly and Lyons [34].

For Rough Transformers, several features of path signatures are important. First, linear functionals on path signatures possess universal approximation properties for continuous functionals.

Theorem A.2. *Fix $T > 0$, and let $K \subset C_b^1([0, T]; \mathbb{R}^d)$. Let $f : K \rightarrow \mathbb{R}$ be continuous with respect to the sup-norm topology on $C_b^1([0, T]; \mathbb{R}^d)$. Then for any $\epsilon > 0$, there exists a linear functional ℓ such that*

$$|f(\overline{X}) - \langle \ell, S(\overline{X})_{0,T} \rangle| \leq \epsilon, \quad (15)$$

for any $\widehat{X} \in K$, where \overline{X} denotes the time-added augmentation of \widehat{X} .

For a proof of A.2, see Arribas [2]. Even though Theorem A.2 guarantees that *linear* functionals are sufficient for universal approximation, linear models are not always sufficient in practice. This motivates the development of nonlinear models built upon the path signature which efficiently extract path behavior.

The second feature is that the terms of the path signature decay factorially, as described by the following proposition.

Proposition A.3. *Given $\widehat{X} \in C_b^1([0, T]; \mathbb{R}^d)$, for any $s, t \in [0, T]$, we have that for any $I \in \mathcal{I}_d^n$*

$$|S(\widehat{X})_{0,T}^I| = O(1/n!). \quad (16)$$

For a proof of Proposition A.3, see [53]. Hence, the number of terms in signature grows exponentially in the level of the signature, but the tail of the signature is well-behaved, so only a few levels in a truncated signature are necessary to adequately approximate continuous functionals.

A.1 Signatures of Piecewise Linear Paths.

In the Rough Transformer, we use linear interpolation of input time-series to get a continuous-time representation of the data. As mentioned in Section 3, the signature computation in this case is particularly simple.

Suppose $\widehat{X}_k : [t_k, t_{k+1}] \rightarrow \mathbb{R}^d$ is a linear interpolation between two points $X_k, X_{k+1} \in \mathbb{R}^d$. That is,

$$\widehat{X}_k(t) = X_k + \frac{t - t_k}{t_{k+1} - t_k} (X_{k+1} - X_k). \quad (17)$$

Then the signature of \widehat{X}_k is given explicitly by

$$S(\widehat{X}_k)_{t_k, t_{k+1}} = \left(1, X_{k+1} - X_k, \frac{1}{2}(X_{k+1} - X_k)^{\otimes 2}, \frac{1}{3!}(X_{k+1} - X_k)^{\otimes 3}, \dots, \frac{1}{n!}(X_{k+1} - X_k)^{\otimes n}, \dots \right), \quad (18)$$

where \otimes denotes the tensor product. Let $\widehat{X}_k * \widehat{X}_{k+1}$ denote the *concatenation* of \widehat{X}_k and \widehat{X}_{k+1} . That is, $\widehat{X}_k * \widehat{X}_{k+1} : [t_k, t_{k+2}] \rightarrow \mathbb{R}^d$ is given by

$$\widehat{X}_k * \widehat{X}_{k+1}(t) = \begin{cases} \widehat{X}_k(t) & t \in [t_k, t_{k+1}] \\ \widehat{X}_{k+1}(t) & t \in (t_{k+1}, t_{k+2}]. \end{cases} \quad (19)$$

The signature of the concatenation $\widehat{X}_k * \widehat{X}_{k+1}$ is given by *Chen's relation*, whose proof is in [53].

Proposition A.4 (Chen’s Relation). *The following identity holds:*

$$S(\widehat{X}_k * \widehat{X}_{k+1})_{t_k, t_{k+2}} = S(\widehat{X}_k)_{t_k, t_{k+1}} \otimes S(\widehat{X}_{k+1})_{t_{k+1}, t_{k+2}}, \quad (20)$$

where for elements $A, B \in T((\mathbb{R}^d))$ with $A = (A_0, A_1, A_2, \dots)$ and $B = (B_0, B_1, B_2, \dots)$ the tensor product \otimes is defined

$$A \otimes B = \left(\sum_{j=0}^k A_j \otimes B_{k-j} \right)_{k \geq 0}. \quad (21)$$

Let $\mathbf{X} = (X_0, \dots, X_L)$ be a time-series. Then the linear interpolation $\tilde{X} : [0, T] \rightarrow \mathbb{R}^d$ can be represented as the concatenation of a finite number of linear paths:

$$\tilde{X} = \widehat{X}_0 * \dots * \widehat{X}_{L-1}. \quad (22)$$

Hence, the signature is

$$S(\tilde{X})_{0, T} = S(\widehat{X}_0)_{0, t_1} \otimes \dots \otimes S(\widehat{X}_{L-1})_{t_{L-1}, T}. \quad (23)$$

B Related Work, Experimental Choices, and Impact Statement

Continuous-time models. Since their introduction in [13], Neural ODEs were extended in various ways to facilitate modelling continuous time-series data [71, 63, 35, 41, 77]. While Neural ODEs and their extensions are successful in certain tasks they are burdened with a high computational cost, which makes them scale very poorly to long sequences in the time-series setting. Various authors propose methods and augmentations to vanilla Neural ODEs to decrease their computational overhead [25, 6]. Other approaches to augmenting deep learning methods to modelling continuous data include implicit neural representations [78, 30] or Fourier neural operators [52, 65].

Transformers. First proposed in [82], the Transformer has been exceptionally successful in discrete sequence modelling tasks such as natural language processing (NLP). Key to the success of the Transformer in NLP is the attention mechanism, which extracts long-range dependencies. There are a number of extensions to improve efficiency and decrease the computation cost of the attention mechanism [51, 84, 24, 43, 17].

Signatures in machine learning. The path signature originates from theoretical stochastic analysis [53]. Now path signatures are a popular tool in machine learning, because they are viewed as an effective feature transformation for sequential data [66, 28, 47]. Signatures are also used to mitigate the computational cost of Neural CDEs in long time-series [60] and non-Markovian stochastic control problems [40]. Other more recent works in this direction include [20, 83]. Randomized signatures [23, 21] and the signature kernel [49, 75] are two approaches which mitigate the curse of dimensionality inherent in the path signature computation. Rough Transformers provide a first step towards incorporating path signatures for continuous-time sequence modelling using Transformers.⁶

Long-Range Sequence modelling. A highly relevant line of research related to enhancing recurrent neural networks’ capability to capture long-term dependencies involves the development of various models. These include Unitary RNNs [1], Orthogonal RNNs [39], expRNNs [50], chronoLSTM [79], antisymmetric RNNs [11], Lipschitz RNNs [26], coRNNs [72], unicoRNNs [73], LEMs [74], waveRNN [45], Linear Recurrent Units [64], and Structured State Space Models [33, 32]. While we utilize many benchmarks and synthetic tasks from these works to test our model, it is important to note that our work is not intended to compete with the state-of-the-art in these tasks. Therefore, we do not directly compare our model with the models mentioned above. Instead, this paper seeks to show that the baseline Transformer architecture can benefit from the use of signatures by (i) becoming more computationally efficient, (ii) being invariant to the sampling rate of the signal, and (iii) having a good inductive bias for temporal and spatial processing. Furthermore, we highlight that RFormer brings alternative benefits, such as the ability to perform spatial processing effectively, which is a setting in which long-range sequence models typically struggle.

⁶For a preliminary version of this paper, we also direct the reader to [59]

Efficient Attention Variants. There are several efficient self-attention variants that have emerged over the years, including Sparse Transformer [15], Longformer [5], Linear Transformers [43], BigBird [87], Performer [17], or Diffuser [27]. In our setting, we highlight that a central part of this paper is to showcase how signatures significantly reduce the computational requirements of vanilla attention, and empirically demonstrate that this also results in improved learning dynamics and invariance to the sampling frequency of the signal. Given the large efficiency gains that we observed with this approach when employed on vanilla attention, we did not consider that further experimentation on other forms of “approximate” attention was needed. Since most variants of attention seek to make the operation more efficient through several approximations (e.g., linearization or sparsification techniques), we believe that a first attempt at showcasing the power of multi-view signatures on vanilla attention is already significant. However, other variants of attention (such as the ones outlined before) could be added on top of the signature representations to obtain even better efficiency gains.

Limitations and Future Work. The experiments and results presented in this paper are constrained by the relatively small scale of the models studied. For example, we consider Transformer with a single head and without extensive hyperparameter tuning. Compared to state-of-the-art models like SSMS, our models may miss out on significant performance enhancements. We do believe that the small-scale experiments carried out in this paper offer other advantages, such as more generalizable results and conclusions and more precise hyperparameter tuning due to a reduced search space. The main objective of this paper was to showcase the benefits of path signatures in the context of Transformers, when compared to its vanilla self-attention variant, making the choice of small-scale experiments both necessary and advantageous. In future research, we could examine the full impact of our findings for the machine learning community and incorporate the core concepts into more advanced sequence modelling architectures.

C Experimental Details

All experiments are conducted on an NVIDIA GeForce RTX 3090 GPU with 24,564 MiB of memory, utilizing CUDA version 12.3. The timings presented in all tables are obtained by executing each model independently for each dataset and averaging the resulting times across 100 epochs. We take down the hyperparameters used in the RFormer model for each of the datasets in the paper, which were chosen in accordance with the performance of the model in the validation set.

Table 5: Hyperparameters validation on the evaluated datasets.

Dataset	Learning Rate	Number of Windows	Sig. Depth	Sig. Type	Univariate/Multivariate Sig.
Sinusoidal	1×10^{-3}	75	2	Multi-View	-
Eigenworms	1×10^{-3}	30	2	Multi-View	Multivariate
LOB (1k)	1×10^{-5}	250	2	Multi-View	Univariate
LOB (20k)	1×10^{-5}	1000	2	Multi-View	Univariate
HR	1×10^{-3}	75	4	Local	Multivariate

To prevent excessive growth in signature terms, we use the univariate signature in LOB datasets. As an alternative, one could employ randomized signatures [21] or low-rank approximations [10, 12].

D Models Validation

This section collects the validation of Step and Depth for the neural RDE model in each of the evaluated datasets. Optimal values are selected for evaluation on test-set. Early-stopping is used with same criteria than [60].

Table 6: Validation accuracy on the sinusoidal dataset.

Acc. Val	Step	Depth	Memory Usage (Mb)	Elapsed Time (s)
17.26	2	2	778.9	6912.7
12.21	2	3	770.3	1194.43
16.35	4	2	382.2	2702.48
19.27	4	3	386.16	574.97
20.99	8	2	193	1321.36
24.02	8	3	194.17	332.17
17.15	16	2	97.13	136.43
21.59	16	3	98.17	156.93
17.46	24	2	65.96	105.94
20.59	24	3	66.68	98.97

Table 7: Validation accuracy on the long sinusoidal dataset.

Acc. Val	Step	Depth	Memory Usage (Mb)	Elapsed Time (s)
11.10	2	2	4017.22	2961.98
9.59	2	3	4008.33	2779.52
10.39	4	2	2001.76	1677.78
10.19	4	3	2006.80	1615.64
14.03	8	2	1004.07	665.55
15.34	8	3	1005.72	723.41
1.61	16	2	503.66	125.85
1.92	16	3	505.28	120.63
1.51	24	2	339.80	58.87
2.12	24	3	341.90	69.35

Table 8: Validation loss on the LOB dataset (1K).

Val Loss	Step	Depth	Memory Usage (Mb)	Elapsed Time (s)
0.58	2	2	1253.55	180.79
1.74	2	3	1447.57	308.52
1.58	4	2	623.87	71.18
32.90	4	3	754.05	87.81
2.94	8	2	317.40	61.27
4.84	8	3	406.88	62.71
2.24	16	2	164.70	18.67
6.26	16	3	234.92	24.20
3.82	24	2	112.80	12.69
15.35	24	3	176.68	14.92

Table 9: Validation accuracy on the EW dataset.

Acc. Val	Step	Depth	Memory Usage (Mb)	Elapsed Time (s)
84.62	2	2	5799.40	21289.99
87.18	2	3	6484.93	25925.80
79.49	4	2	2891.61	11449.14
82.05	4	3	3240.99	9055.12
82.05	8	2	1446.94	4143.26
76.92	8	3	1624.73	3616.43
82.05	16	2	724.35	1909.69
76.92	16	3	817.04	1924.27
79.49	24	2	483.92	1098.21
74.36	24	3	543.78	987.02

Table 10: Validation loss on the HR dataset.

Acc. Val	Step	Depth	Memory Usage (Mb)	Elapsed Time (s)
2.44	2	2	5044.44	56492.33
3.03	2	3	5059.28	39855.19
3.67	4	2	2515.40	10765.58
16.04	4	3	2531.44	7157.20
5.35	8	2	1259.30	3723.94
2.70	8	3	1268.60	18682.82
3.58	16	2	632.08	3518.96
3.64	16	3	636.64	7922.96
3.86	24	2	422.74	3710.95
3.55	24	3	426.83	6567.02

E Ablation Studies

E.1 Global and Local Signature Components

In this section, we ablate the use of the multi-view signature transform over both global and local transformations of the input signal. The results are shown in Figure 5 for the sinusoidal datasets and Table E.1 for the remaining datasets. In most cases, the use of local and global components enhances the performance of RFormer. This choice, however, can be seen as a hyperparameter and will be dataset-dependent.

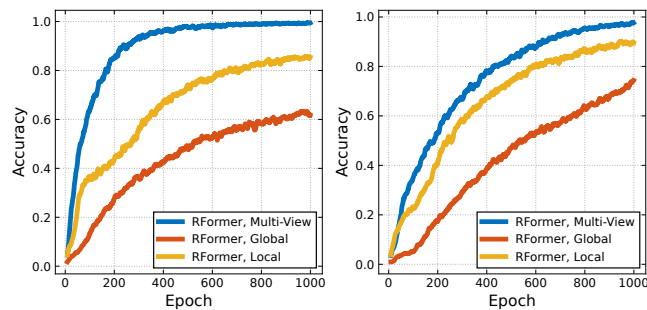


Figure 5: Ablation of local and local components of the multi-view signature for the sinusoidal datasets.

Table 11: Test performance (mean \pm std), computed across five seeds for all datasets, detaching local and global components of the signature computation.

Model				
	EW (%) \uparrow	HR \downarrow	LOB 1k \downarrow	LOB 20k \downarrow
Local	84.61 \pm 3.62	2.66 \pm 0.21	39.16 \pm 0.61	38.73 \pm 0.41
Global	89.23 \pm 4.10	4.94 \pm 0.44	39.01 \pm 0.24	39.10 \pm 0.36
Multi-View	90.24 \pm 2.15	4.38 \pm 0.17	38.81 \pm 0.19	38.44 \pm 0.15

E.2 Signature Level and Naive Downsampling

One of the main points of the paper is that the shorter representation of the time-series endowed by the signatures helps to significantly reduce the computational cost of the self-attention operation with minimal information loss (and with improved performance in many of the experiments). By equation (18), one sees that the first level of the signature of a linear function is the difference between its endpoints. Hence, using multi-view attention with signature level one operates on the increments of piecewise-linear interpolated data, which corresponds to naive downsampling. To test that higher levels of the signature provide improvements in performance, we compare the result of using the signature on the datasets tested in Table 12 below.

Table 12: Comparative performance of different methods on datasets.

Dataset	Linear-Interpolation + Vanilla	Rough Transformer with sig level (n)	Improvement
EigenWorms	64.10%	90.24% (2)	40.77%
HR	10.56	2.66 (4)	74.81%

Clearly, there is a significant performance gain in considering higher levels of the signature because one can capture the higher-order interactions between the different time-series.

F Additional Experiments and Comparisons

F.1 Random Drop Experiments

Furthermore, we conduct a new set of experiments in which we dropped 30% and 70% of the dataset for RFormer. Note that even with a 70% drop rate in the EigenWorms dataset, the vanilla Transformer fails to run due to memory limitations. Therefore, to provide results for the Transformer model on the EigenWorms dataset, we conduct experiments with an 85% drop rate. This comparison highlights the performance gap between the vanilla Transformer and our proposed model under these conditions, with the RFormer model yielding superior results. All results are computed across five seeds, and are summarized in the tables and figure below.

Table 13: Performance of models under various data drop scenarios for EW dataset.

Model	Full	30% Drop	50% Drop	70% Drop	85% Drop
Transformer	OOM	OOM	OOM	OOM	72.45% \pm 3.36
RFormer	90.24% \pm 2.15	87.86% \pm 3.28	87.69% \pm 4.97	83.35% \pm 2.86	82.74% \pm 2.13

Table 14: Performance consistency of RFormer under data drop scenarios for HR dataset.

Model	Full	30% Drop	50% Drop	70% Drop
RFormer	2.66 \pm 0.21	2.72 \pm 0.19	2.82 \pm 0.05	2.98 \pm 0.08

Table 15: Epoch-wise performance under different data drop scenarios for the sinusoidal dataset.

	Epoch 100	Epoch 250	Epoch 500	Epoch 1000
30% Drop	48.6%	82.5%	91.4%	99.3%
70% Drop	35.7%	56.8%	64.9%	67.8%

Table 16: Epoch-wise performance under different data drop scenarios for the long sinusoidal dataset.

	Epoch 100	Epoch 250	Epoch 500	Epoch 1000
30% Drop	39.1%	72.6%	96.2%	98.2%
70% Drop	27.5%	66.7%	78.5%	85.3%

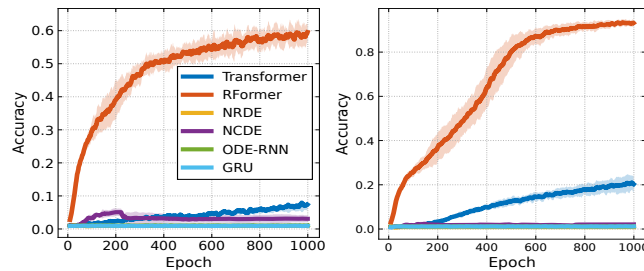


Figure 6: Test accuracy per epoch for the frequency classification task across three random seeds for sinusoidal datasets with 50% random drop per epoch. **Left:** Sinusoidal dataset. **Right:** Long Sinusoidal dataset.

F.2 Additional Efficiency Experiments and Discussion

We conduct additional experiments investigating Rough Transformers’ runtime compared with other models, see Table 17 for a summary of the results. In this experiment, we use the synthetic sinusoidal dataset considered in our paper and computed the runtime per epoch for varying sequence lengths. We demonstrate results for two variants of RFormer: “online”, which corresponds to computing the signatures of each batch during training (resulting in significant redundant computation), and “offline”, which corresponds to computing the signatures in one go at the beginning of training. We also include a recent RNN-based model as a basis for comparison with high-performing RNN baselines.

Table 17: Seconds per epoch for growing input length and for different model types on the sinusoidal dataset.

Model	S/E for Varying Context Length ↓							
	L=100	L=250	L=500	L=1000	L=2500	L=5000	L=7.5k	L=10k
ContiFormer	61.36	248.31	1165.02	OOM	OOM	OOM	OOM	OOM
Transformer	0.75	0.79	0.82	0.95	1.36	5.31	9.32	16.32
RFormer (Online)	0.75	0.88	0.94	1.03	1.28	1.55	1.83	2.35
RFormer (Offline)	0.67	0.64	0.63	0.65	0.60	0.59	0.62	0.60
NRDE	5.87	11.67	20.27	44.01	103.11	201.21	312.31	467.47
NCDE	42.59	121.82	225.14	458.09	1126.77	2813.42	4199.50	5345.39
GRU	1.56	1.55	1.65	1.63	1.78	2.37	3.65	4.79

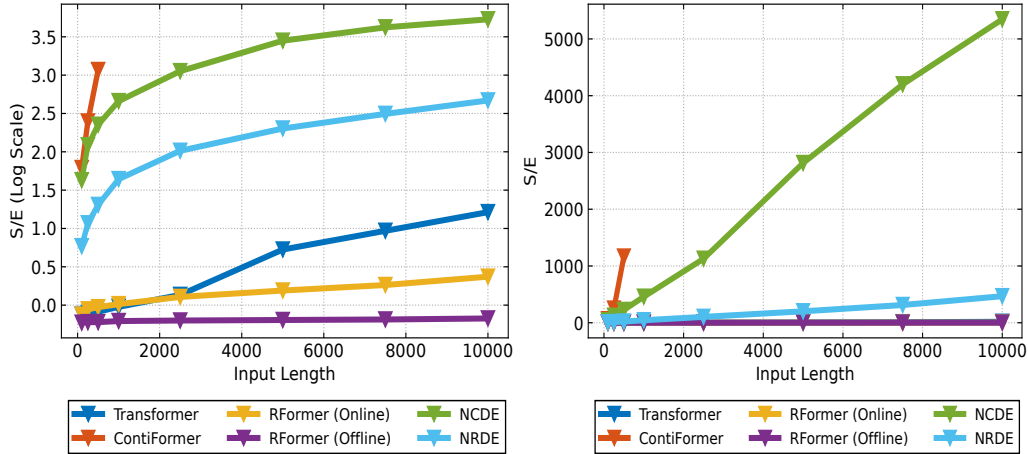


Figure 7: Seconds per epoch for growing input length and for different model types on the sinusoidal dataset. **Left:** Log Scale. **Right:** Regular Scale.

We remark that previous running times are obtained with a batch size of 10. Further, the `ContiFormer` model could be run for $L = 1000$ if decreasing the batch size to 2 (which significantly affects the parallelization process), avoiding OOM issues and resulting in 4025 seconds/epoch, which is several orders of magnitude larger than `RFormer`. As an additional experiment, we tested the epoch time (S/E) of `RFormer` for extremely oversampled sinusoidal time series. We show our results in the table below.

Table 18: Seconds per epoch for very large input length.

Model	S/E for Varying Context Length ↓			
	L=25k	L=50k	L=100k	L=250k
RFormer (Online)	5.39	9.06	19.95	45.20
RFormer (Offline)	0.60	0.61	0.60	0.63

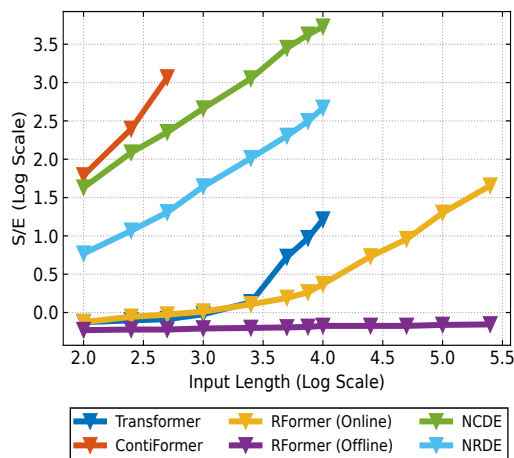


Figure 8: Seconds per epoch for long inputs (on a log-log scale) and for different model types on the sinusoidal dataset.

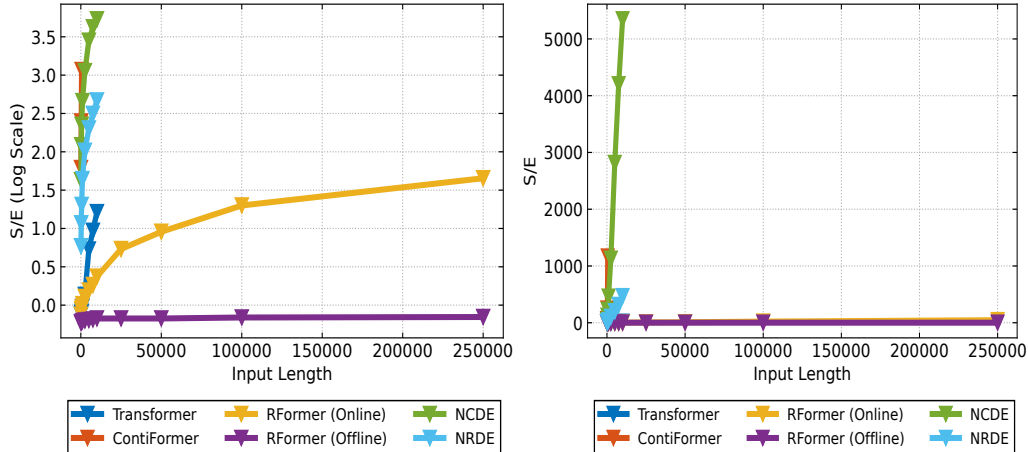


Figure 9: Seconds per epoch for long inputs (at different scales) and for different model types on the sinusoidal dataset. **Left:** Log Scale. **Right:** Regular Scale.

To implement the signature computation, we use on the `iisignature` package [70], which is designed to take advantage of properties of the signature (like Chen’s identity) to yield fast computations. To test this empirically, we measure the computational time of the multi-view signature operation for all datasets used in the paper (with the same window size and signature depth). Table 19 reports the results.

Table 19: Dataset processing times for training, validation, and testing phases.

Dataset	Train	Val	Test
Eigenworms	1.11 s.	0.19 s.	0.19 s.
HR	4.23 s.	0.84 s.	0.85 s.
LOB (1k)	1.69 s.	0.32 s.	0.32 s.
LOB (20k)	0.267 s.	0.016 s.	0.016 s.

Thus, the time needed to compute the signature is inconsequential when compared with the time required to train standard models on the full or even downsampled datasets, since this step has to be carried out only once. To put this into context with an example, we note that it takes 4s to compute the signature representations for the HR dataset (which is about half the time it takes for the Vanilla Transformer to go through one epoch) and results in a $26\times$ increase in computational speed for RFormer when compared to the vanilla Transformer.

To showcase that this is the case for not only sequences of moderate length, but also extremely long sequences, we also carry out the following experiment where we compute the signature representation for the sine dataset, with a progressively increasing number of datapoints. As seen in the following table, this does not cause an explosion in computational time:

Table 20: Processing times for different sizes on the sinusoidal dataset.

Size	100	250	500	1k	2.5k	5k	7.5k	10k	25k	50k	75k	100k
Time	0.15 s	0.21 s	0.24 s	0.39 s	0.42 s	0.51 s	0.70 s	1.09 s	1.64 s	2.94 s	4.49 s	5.74 s

Finally, Table 21 summarises the seconds per epoch for all models considered. It shows that RFormer is competitive when modelling datasets with extremely long sequences (such as EW and the long LOB dataset) without an explosion in the memory requirements. RFormer exploits the parallelism of the attention mechanism to significantly accelerate training time, as the length of the input sequence is decreased substantially. In particular, we observe speedups of $1.4\times$ to $26.11\times$ with respect to standard attention, and higher when compared with all methods requiring numerical solutions to ODEs.

Table 21: Seconds per epoch for all models considered.

Model	Running Time (seconds / epoch)				
	Sine	EW	LOB (1k)	LOB (20k)	HR
GRU	0.12	<u>0.25</u>	<u>0.05</u>	<u>0.61</u>	<u>1.07</u>
ODE-RNN	5.39	48.59	2.66	127.59	50.71
Neural CDE	9.83	-	4.92	-	-
Neural RDE	0.85	5.23	12.00	118.40	9.52
Transformer	0.77	OOM	0.07	OOM	11.71
RFormer	<u>0.55</u>	0.11	0.04	0.07	0.45
Speedup	1.4×	-	1.75×	-	26.11×

F.3 Additional ContiFormer Comparisons

Also, to provide some context of the performance of ContiFormer compared with our method (and not only results on complexity and training times), we run the model on the sinusoidal classification task for signals of length $L = 100$ and $L = 250$. Due to the slow running time of the ContiFormer model, we did not consider sequence lengths of $L > 250$. We evaluate the ContiFormer model using one head. However, given the subpar results we obtain, we also test it with four heads, using the hyperparameters originally used in the paper for their irregularly sampled time series classification experiments. By contrast, all variations of RFormer tested in this paper employ only one head, but reported significantly better results.

Table 22: Model performance for $L = 100$.

Model	Epoch 100	Epoch 250	Epoch 500
ContiFormer (1 Head)	2.3%	2.8%	3.1%
ContiFormer (4 Heads)	8.5%	17.3%	20.0%
Transformer (1 Head)	13.7%	40.1%	82.8%
RFormer (1 Head)	38.7%	81.1%	92.3%

Table 23: Model performance for $L = 250$.

Model	Epoch 100	Epoch 250	Epoch 500
ContiFormer (1 Head)	2.7%	2.7%	4.2%
ContiFormer (4 Heads)	11.4%	18.1%	20.2%
Transformer (1 Head)	3.2%	20.4%	62.9%
RFormer (1 Head)	46.5%	84.2%	94.2%

F.4 Experiments on Spatio-Temporal Interactions

Aside being able to capture long-range temporal interactions, we hypothesize that RFormer can capture spatial dependencies between different channels in the time series better. To test this out, we construct a synthetic experiment for a 2-channel time series, where each channel contains a time series of the form $\sin(\omega_i t + \nu_i)$, $i = \{1, 2\}$ for ω_i and ν_i randomly sampled in the interval $[0, 2\pi]$. For half of the data sampled, the last 1% of temporal samples in both channels are the same. The task is to classify if the samples in that final interval are the same, see Figure 10.

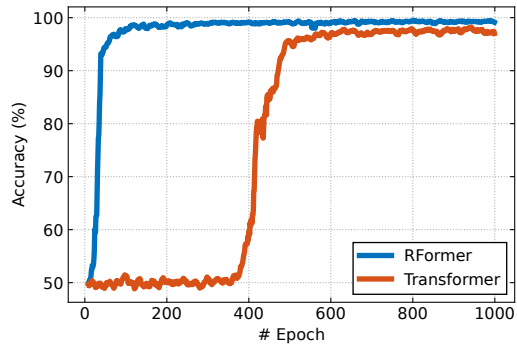


Figure 10: Accuracy of RFormer and Transformer in the spatial sinusoidal classification task.

Thus, RFormer can capture the spatial interactions much better than the vanilla Transformer model, showcasing the ability of signatures to capture higher-order interactions between different temporal channels. We highlight that other approaches in the literature have employed graphs as a means with which to model spatial information in time series, see [18, 54], in particular, those employing latent graph inference [44, 7, 19] to find the structure connecting different channels in a differentiable manner.